NANO LETTERS

LETTER

pubs.acs.org/NanoLett

Two-Photon 3D FIONA of Individual Quantum Dots in an Aqueous Environment

Ruobing Zhang,[†,‡,▽] Eli Rothenberg,[‡,§,○,▽] Gilbert Fruhwirth,[∥] Paul D. Simonson,[‡,§] Fangfu Ye,[‡,§] Ido Golding,[‡,§,⊥] Tony Ng,[∥] Ward Lopes,[‡,#] and Paul R. Selvin[*,†,‡,§]

[†]Center for Biophysics and Computational Biology, [‡]Center of Physics of Living Cells, and [§]Physics Department, and University of Illinois at Urbana−Champaign, Urbana, Illinois 61801, United States

[∥]The Richard Dimbleby Department of Cancer Research, Randall Division of Cell & Molecular Biophysics, and Division of Cancer Studies, King's College London, London WC2R 2LS, United Kingdom

[⊥]Verna and Marrs McLean Department of Biochemistry and Molecular Biology, Baylor College of Medicine, Houston, Texas 77030, United States

[#]Physics Department, Williams College, Williamstown, Massachusetts 01267, United States

Supporting Information

ABSTRACT: We report the first two-photon (2P) microscopy of individual quantum dots (QDs) in an aqueous environment with both widefield and point-scan excitations at nanometer accuracy. Thiol-containing reductants suppress QD blinking and enable measurement of the 36 nm step size of individual Myosin V motors in vitro. We localize QDs with an accuracy of 2−3 nm in all three dimensions by using a 9 × 9 matrix excitation hologram and an array detector, which also increases the 3D scan imaging rate by 80-fold. With this 3D microscopy we validate the LamB receptor distribution on *E. coli* and the endocytosis of EGF-receptors in breast cancer cells.

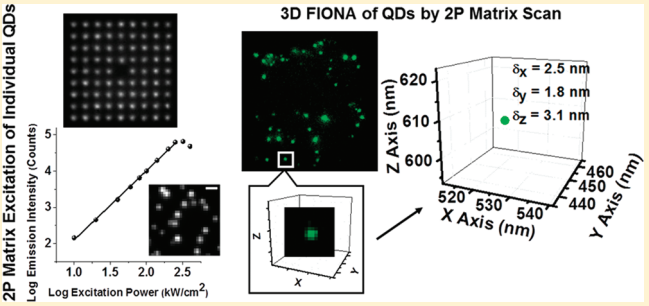

KEYWORDS: Two photon, quantum dot, FIONA, holographic excitation, breast cancer, EGFR

One-photon (1P) microscopy of individual quantum dots (QDs) has become routine.[1−3] In contrast, two-photon (2P) microscopy of individual QDs has not had the same success despite the many advantages that 2P microscopy offers: reduced scattering, deep sample penetration, and intrinsic confocality when excited with point excitation.[4] 2P microscopy of ensembles of QDs in aqueous samples has been achieved by Larson et al. in 2003.[5] They showed QDs had large absorption cross sections under 2P scan excitation. Nevertheless, individual 2P QD-microscopy has been possible only in artificial environments, such as air-dried samples of QDs,[6] or at cryogenic temperatures.[7] 2P microscopy of individual organic-based fluorophores has also been problematic since most fluorophores have very small 2P absorption cross sections, as well as poor photostability.[8,9]

Here we report the application of 2P microscopy to individual QDs in a biological setting with nanometer spatial accuracy in three dimensions, both in solution and in live and fixed cells. We call our technique two-photon fluorescence imaging with one nanometer accuracy (2P FIONA), in analogy with the one-photon technique.[10] With 2P excitation, we are able to achieve three-dimensional (3D) nanometer spatial accuracy, as opposed to the two-dimension FIONA previously achieved with one photon microscopy.[10] We also introduce a fast imaging method using a holographic matrix in excitation and EMCCD in detection that achieves an 80-fold improvement in speed and reduces spherical aberrations.

We first imaged immobilized single QDs in an aqueous buffer via a widefield 2P microscope (Figure 1, "widefield" path, and Figure 2a). Ordinarily, a scanning system is used in 2P microscopy of regular organic fluorophores. However, widefield microscopy is possible with QDs because their 2P excitation is extremely efficient. The log emission intensity versus log excitation power plot indicates the I^2 dependence of 2P excitation (Figure 2b). At a 2P excitation flux of ≥250 kW/cm^2, saturation begins to take place, accompanied by significant photobleaching. The photobleaching occurs at the power about 20 times lower than the 2P excitation levels reported for organic dyes.[4,5] Furthermore, the addition of small thiols into the buffer, as has been observed for 1P excitation,[11] is very helpful. Dithiothreitol (DTT, MW = 154, 1−100 mM) or β-mercaptoethanol (BME, MW = 78, 1−10%) results in nearly complete (>90%) suppression of blinking (Figure 2c). Without reductants present, the

Received: April 12, 2011
Revised: August 18, 2011
Published: September 02, 2011

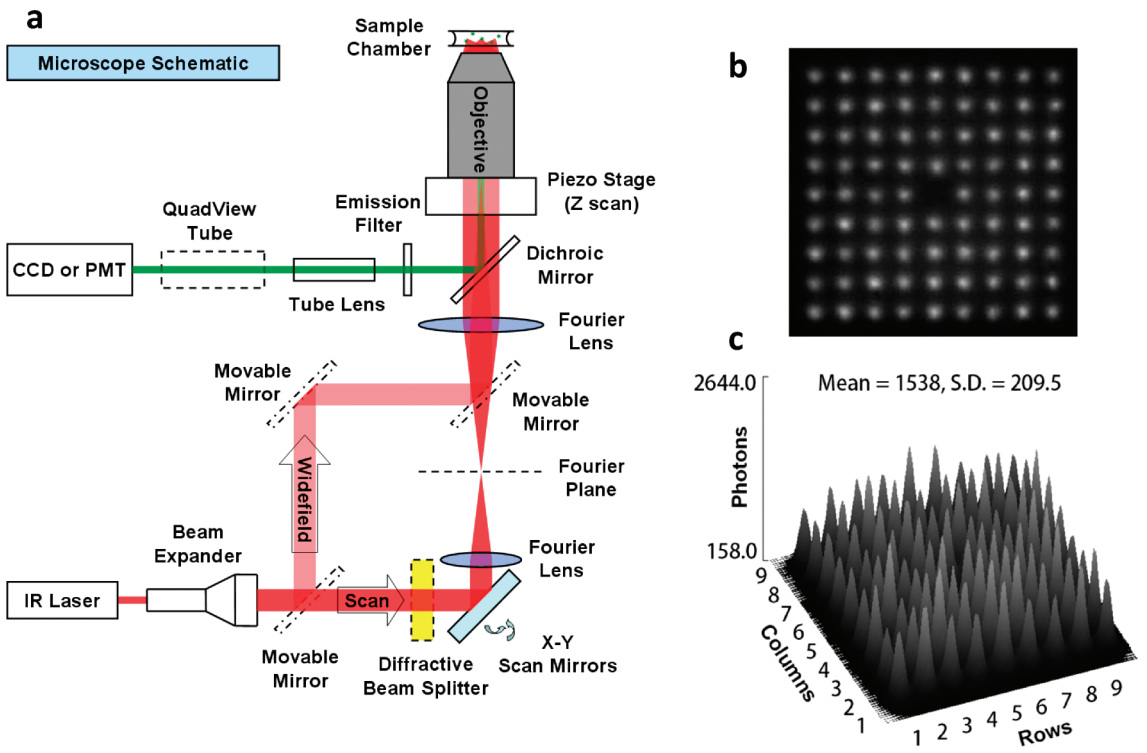

Figure 1. Configuration of the 2P microscope. (a) Widefield and single- and multipoint scan. In the sample chamber a 3 × 3 matrix, instead of the actual 9 × 9 matrix is illustrated for clarity. The holograph splitter is conjugated via two 4f lenses to the back focal plane of the objective. (b) Image of excitation hologram matrix. Taken with 1 μM Qdot 605, laser at 785 nm. (c) 2D intensity plot of the hologram matrix in (b): SD = 13.6%.

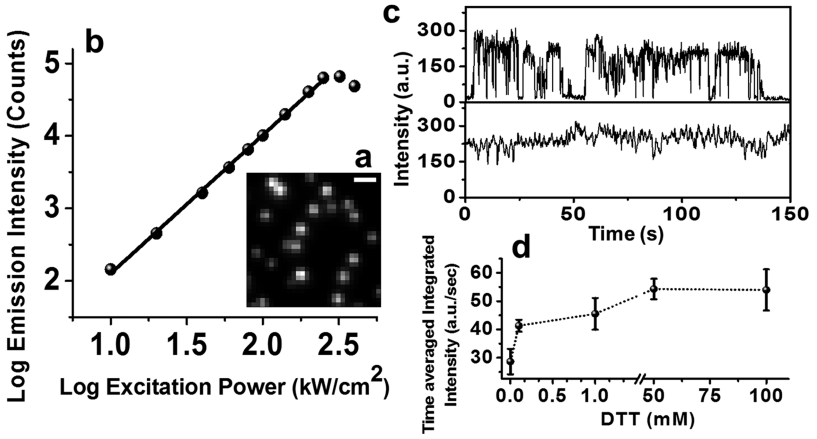

Figure 2. Two-photon excitation response of quantum dots. (a) An image of 2P excited individual QD525. Scale bar is 500 nm. QDs were conjugated to streptavidin and tethered to a BSA−biotin coated surface. Imaging buffer (DPBS, pH7.5) was supplemented with 50 mM DTT. (b) The log average emission intensity of individual QDs plotted versus log excitation power. Slope of linear fit is 1.93, indicating QDs have a predominant quadratic dependence of fluorescence on laser power, in agreement with quadratic power law dependence of two-photon excitation. At higher two-photon excitation power QDs emission is saturated and fast photobleaching occurs. (c) Blinking is near completely eliminated by adding in 50 mM DTT. (d) DTT enhances the QD emission more as its concentration increases.

QDs tend to blink extensively. However, the blinking does prove that they are single QDs (see Supplementary Movie 1, Supporting Information). Larger molecular weight reductants (e.g., glutathione, MW = 307) did not have this effect. Figure 2d shows the effect of DTT on the averaged emission intensity of >100 individual QDs, where an increase in DTT concentration clearly results in an increase in average emission intensity due to suppression of blinking and elimination of nonemitting "off" states. The QDs could also be conveniently used for multicolor detection with a single 2P excitation, just as is true with 1P excitation. The excitation spectra, ranging from 760 to 1000 nm of three different QDs samples with peak emissions at 525, 585, and 655 nm, displayed highly efficient excitation from 760 to 900 nm (Figure S1, Supporting Information).

With blinking suppressed, QDs under 2P widefield excitation have continuous emission and can be used for tracking of biomolecular

dx.doi.org/10.1021/nl201225r |*Nano Lett.* 2011, 11, 4074–4078

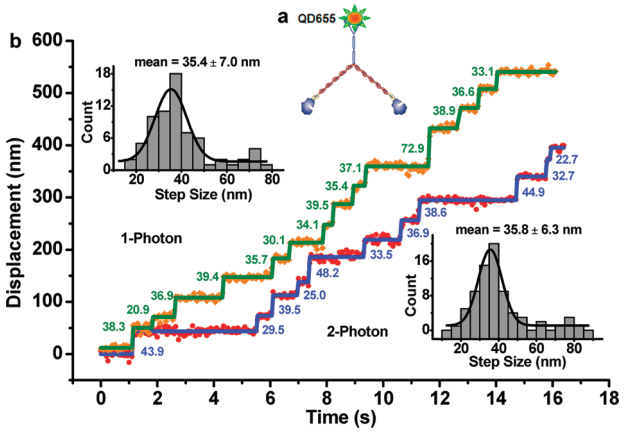

Figure 3. 2P widefield excitation resolves Myosin V step sizes at nanometer accuracy. (a) Labeling of dimeric myosin V construct. (b) Displacements of myosin V motors resolved at 50 ms temporal and one nanometer spatial resolutions under 1P (orange dots, green lines) and 2P (red dots, blue lines) excitation. Step sizes are determined by Student's *t* test, and the step size distribution is fit to a Gaussian fit to give 35.4 ± 7.0 and 35.8 ± 6.3 nm for 1P and 2P widefield imaging, respectively.

motion at nanometer accuracy. We have analyzed a molecular motor, a dimerized myosin V, by placing a QD (655 nm) on the C-terminus (Figure 3a) and exciting it with either 1P or 2P widefield excitation. We expected the step size to be ~36 nm based on previous results from optical trapping[12] and 1P-FIONA data.[10] At 30 ms exposure time, under 2P widefield excitation at 200 kW/cm^2, we detected ~25000 photons and achieved 0.9 nm accuracy; under 1P widefield excitation at 0.4 kW/cm^2, we detected ~20000 photons and achieved 1.1 nm. Figure 3b shows myosin V walking with 2 μM ATP, integrated every 50 ms, and excited with either 1P or 2P excitation. With 1P, we measured the step size of the motor to be 35.4 ± 7.0 nm; with 2P, we measured 35.8 ± 6.3 nm. These results are in excellent agreement with each other and consistent with the expected value. The motor protein stepping rate is evidently not affected by the strong IR power used in 2P excitation, indicating that the laser field does not harm the ATPase activity of myosin V. We also note that total internal reflection (TIR) or near-TIR[13,14] was not required here because of the exceptional brightness and signal-to-noise of the QDs. Nevertheless, single QDs could be excited and imaged with 2P-TIR (Figures S2 and S4, Supporting Information), confirming the high absorption cross section of QDs under 2P.

Widefield illumination, however, does not give *z*-axis discrimination. To achieve this, we used either single-point or multiple-point scanning excitation where the beam(s) was focused to a (near) diffraction-limited focal spot(s). By adding in a holographic beam splitter (Holo/Or Ltd., Israel) into the beam path, we split the beam and generated a 9 × 9 matrix of 80 diffraction-limited focal spots for excitation (See "Scan" excitation path in Figure 1; the central spot is missing, yielding 81 − 1 = 80 spots). The single- or multiple-point was raster scanned in the usual fashion—by a pair of motorized mirrors in *x* and *y* directions and by a piezo-stage mounted under the objective in the *z* axis. We found this considerably simplified the optics compared with the moving mirrors[15,16] or rotational microlenses[17] used previously. Our system could also be easily integrated into current single-point scan microscopes, and its imaging area coverage was conveniently adjustable by changing the conjugation lenses magnification. At the sample, the 80 spots were separated 1.5 μm apart with the 100× objective and quite uniform in terms of power distribution (standard deviation is 6%), leading to very small localization accuracy errors. (See Supporting Information.) In most experiments, we scanned at 100 nm steps in all three dimensions. Moreover, to acquire the simultaneous emission excited by the multiple focal spots, we used an array detector, i.e., an EMCCD camera. The effective pixel size of the EMCCD after magnification was also 100 nm. This holographic matrix (HM) scan technique leads to an 80-fold improvement over single-point scan imaging speed (assuming, of course, that you are imaging the area covered by the matrix). Furthermore, given the brightness of QDs under 2P excitation, the imaging time is also relatively fast. In our cell imaging experiments (see below), for example, a 3D scan requires only 1−3 s or even subsecond depending on the scan step dwell time, while the traditional single-point 2P scan microscope based on organic fluorophores often takes tens of minutes. For example, we applied 3D scanning microscopy to live *E. coli* cells, of which the LamB receptors (binding targets of bacteriophage λ) were labeled with QD605 (Figure 4a).[18,19] *E.coli* cells' viability was not perturbed by the 2P excitation as evidenced by the division of some cells after imaging. The image revealed spatial helices or bands of the receptors on the *E. coli* membrane. The breast cancer cell, another example of the multipoint scanning (Figure 4c), is discussed below.

We are also able to produce three-dimensional FIONA, instead of the usual two-dimensional *x*−*y* FIONA. In part, this is because of the inherent confocality of scanning 2P excitation. In 2D FIONA, one takes a diffraction-limited spot in one image and fits it with a 2D Gaussian in the *x*−*y* plane. The accuracy of locating the center is determined by the equation derived by Thompson et al.,[20] approximately equal to the width of the Gaussian distribution divided by the square-root of the number of photons.[10,20] This yields nanometer accuracy in *x* and *y*. To get nanometer accuracy in the *z* dimension, we took a series of *x*−*y* scan images along *z*; *z* localization can then be determined by fitting *x*−*z* or *y*−*z* PSFs (which should yield the same value) (Figure S3, Supporting Information). Alternatively, a three-dimensional PSF can be constructed and the *x*, *y*, and *z* positions can be resolved, as well as localization accuracies (Figure 4b). We scanned every 100 nm in *z* so the effective pixelation in *z* was 100 nm, the same as in *x* and *y*. (For a more detailed description of 3D FIONA, see Methods and Figure S3 in the Supporting Information.)

As an example, we analyzed single QDs in a basal breast cancer cell line (MDA-MB-468) imaged with 2P in 3D with the holographic approach. The QDs are attached to the epidermal growth factor (EGF) and bound to ErbB1, its EGF-receptor (EGFR), which resides mostly at the plasma membrane of resting cells and is involved in cell proliferation. EGFR is a major drug target of for the treatment of various types of breast cancer. Mutations in EGFR have been found to be involved in unlicensed growth of malignant tumor cells.[21−23] If activated by EGF treatment at 37 °C for 10−30 min, EGFRs are activated, followed by receptor endocytosis showing up under different *z*-slices.[24] We first treated the breast cancer cells with 4 nM QD605-EGF conjugates to trigger EGFR activation and internalization. Then we fixed the cells and mounted them with CyGEL. 1P imaged via TIR showed large autofluorescence (S/N = 1), which was significantly reduced by 2P scanning (S/N = 5) (Figure S4, Supporting Information), in which individual QD-labeled EGFRs were clearly resolved (Figure 4c and Figure S4 in the Supporting

dx.doi.org/10.1021/nl201225r |*Nano Lett.* 2011, 11, 4074–4078

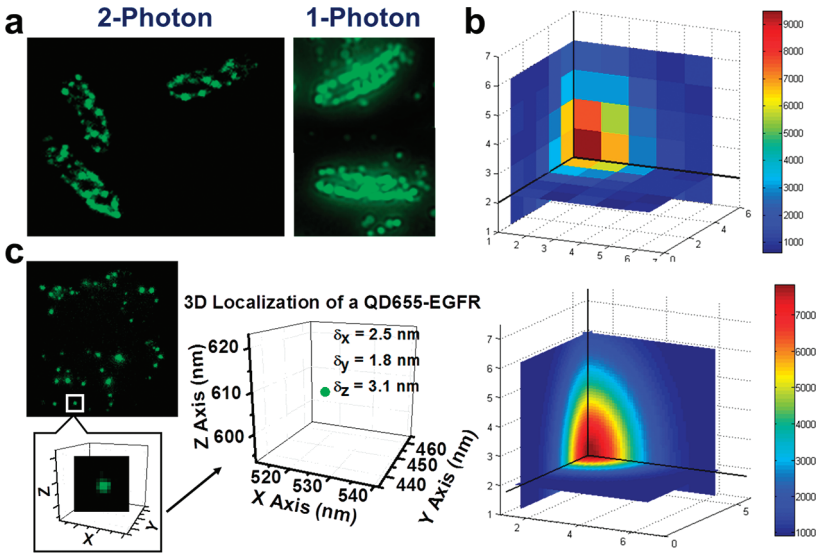

Figure 4. 3D cell imaging by 2P holographic scan of QDs and 3D FIONA. (a) 2P images of live *E. coli* cells reveal helical stripes of QD (605 nm) labeled LamB receptor distribution on the cell membrane. 2P holographic matrix scan images yield better resolution than 1P widefield images. (b) Three-dimensional (3D) FIONA fitting (bottom) of a 3D fluorescent spot localizes the center of it to 2−3 nm accuracy. Cross sections in three perpendicular planes passing the center of the spot are drawn. (c) A QD655-labeled EGF receptor in a breast cancer cell localized in 3D, showing it is on the membrane of the cell. Average z accuracy is slightly lower than x and y accuracies.

Information). (It is therefore unlikely that a scanning-disk 1P-confocal microscope would reduce the autofluorescence enough to achieve the high signal-to-noise measured here with 2P microscopy.) A 3D image of an EGF-QD605 labeled breast cancer cell could be obtained within seconds (1−3 s) for holographic imaging, or even subsecond, depending on the residence time on each pixel (A 3D movie is available as Supplementary Movie 2 in the Supporting Information.) In contrast, regular single-point scanning took one to a few minutes. The plotted data point in Figure 4c shows the 3D position of a QD-labeled EGFR endosome in a representative breast cancer cell, localized at 2.5, 1.8, and 3.1 nm accuracies in x, y, and z, respectively. The z accuracy is slightly lower than x/y accuracies, which is expected because the PSF is slightly larger in the z dimension compared to the $x-y$ dimension. Nevertheless, this indicates that we can achieve <3 nm accuracy in all three dimensions. As expected, the localization showed that receptors were internalized post-EGF treatment. For EGFR dimer or oligomers, as they are smaller than the diffraction limit, we localize the center of the EGFR aggregation either on membrane or in cytoplasm. Stoichiometry and spatial organization of EGFRs in one aggregation require a super-resolution method to resolve, which will be discussed in a future publication.

In conclusion, we report two-photon excitation of individual QDs at room temperature in biological environments both in vitro and in vivo and present a holographic type of scanning technique that improves the imaging rate by 80-fold. 3D nanometer localization accuracy can be obtained from the holographic scan data. The 2P-QD imaging system can easily integrate into conventional scan microscopy due to its simplicity and modularity. The technique opens a way to look inside the live or fixed cells and tissues at single molecule level and nanometer resolution.

■ ASSOCIATED CONTENT

Ⓢ Supporting Information. Materials and methods include preparation of sample and imaging chambers, configurations of widefield and single- and multipoint scan microscopies, labeling of dimeric Myosin V, construct, preparation, and imaging of QD-labeled live *E. coli* and fixed breast cancer cell samples, analysis of stepping, and obtaining three-dimensional FIONA by 3D Gaussian and virtual $x-y/y-z$ images; supplementary figures include QD excitation spectra, simultaneous multicolor imaging of multi-QD labeled live *E. coli* cells, 2P-TIR image of QD, and 3D FIONA schematic. This material is available free of charge via the Internet at http://pubs.acs.org.

■ AUTHOR INFORMATION

Corresponding Author

*E-mail: selvin@uiuc.edu.

Present Addresses

○Department of Biochemistry, New York University School of Medicine, 550 First Ave., MSB 363, New York, NY 10016.

Author Contributions

▽Equal contribution.

■ ACKNOWLEDGMENT

This work was supported to P.R.S. by NIH Grant GM086214 and by NSF Grants (DBI 0649779 and EAGER 0968976 with W. L.; and 082265 with I.G.); to I.G. by NIH Grant R01GM082837 and HFSP Grant RGY 70/2008; and to T.N. by CR-UK & EPSRC, in association with the MRC and DoH, via the KCL-UCL Comprehensive Cancer Imaging Centre, C1519/A10331. We appreciate the Lee Sweeney's lab at the University of Pennsylvania for providing the Myosin V HMM construct and Samuel Skinner for help with the 1P imaging of *E. coli*.

■ REFERENCES

(1) Chan, W. C. W.; Nie, S. *Science* **1998**, *281* (5385), 2016–2018.

(2) Dahan, M.; Lévi, S.; Luccardini, C.; Rostaing, P.; Riveau, B.; Triller, A. *Science* **2003**, *302* (5644), 442–445.
(3) Michalet, X.; Pinaud, F. F.; Bentolila, L. A.; Tsay, J. M.; Doose, S.; Li, J. J.; Sundaresan, G.; Wu, A. M.; Gambhir, S. S.; Weiss, S. *Science* **2005**, *307* (5709), 538–544.
(4) Denk, W.; Strickler, J. H.; Webb, W. W. *Science* **1990**, *248* (4951), 73–76.
(5) Larson, D. R.; Zipfel, W. R.; Williams, R. M.; Clark, S. W.; Bruchez, M. P.; Wise, F. W.; Webb, W. W. *Scicence* **2003**, *300* (5624), 1434–1436.
(6) Rothenberg, E.; Ebenstein, Y.; Kazes, M.; Banin, U. *J. Phys. Chem. B* **2004**, *108* (9), 2797–2800.
(7) Verberk, R.; Oijen, A. M. v.; Orrit, M. *Phys. Rev. B* **2002**, *66* (23), 233202.
(8) Sanchez, E. J.; Novotny, L.; Holtom, G. R.; Xie, X. S. *J. Phys. Chem. C* **1997**, *101* (38), 7019–7023.
(9) Mertz, J.; Xu, C.; Webb, W. W. *Opt. Lett.* **1995**, *20* (24), 2532–2534.
(10) Yildiz, A.; Forkey, J. N.; McKinney, S. A.; Ha, T.; Goldman, Y. E.; Selvin, P. R. *Science* **2003**, *300*, 2601–2605.
(11) Hohng, S.; Ha, T. *J. Am. Chem. Soc.* **2004**, *126* (5), 1324–1325.
(12) Mehta, A. D.; Rock, R. S.; Rief, M.; Spudich, J. A.; Mooseker, M. S.; Cheney, R. E. *Nature* **1999**, *400*, 590–593.
(13) Kural, C.; Kim, H.; Syed, S.; Goshima, G.; Gelfand, V. I.; Selvin, P. R. *Science* **2005**, *308* (5727), 1469–1472.
(14) Tokunaga, M.; Imamoto, N.; Sakata-Sogawa, K. *Nat. Methods* **2008**, *5* (2), 159–161.
(15) Nielsen, T.; Fricke, M.; Hellweg, D.; Andresen, P. *J. Microsc.* **2001**, *201* (3), 368–376.
(16) Niesner, R.; Andresen, V.; Neumann, J.; Spiecker, H.; Gunzer, M. *Biophys. J.* **2007**, *93* (7), 2519–2529.
(17) Bewersdorf, J.; Pick, R.; Hell, S. W. *Opt. Lett.* **1998**, *22* (9), 655–657.
(18) Schwartz, M. *Methods Enzymol.* **1983**, *97*, 100–112.
(19) Oddershede, L.; Dreyer, J. K.; Grego, S.; Brown, S.; Berg-Sørensen, K. *Biophys. J.* **2002**, *83* (6), 3152–3161.
(20) Thompson, R. E.; Larson, D. R.; Webb, W. W. *Biophys. J.* **2002**, *82* (5), 2775–2783.
(21) Lurje, G.; Lenz, H. J. *Oncology* **2009**, *77*, 400–410.
(22) Engelman, J. A.; Janne, P. A. *Clin. Cancer Res.* **2008**, *14* (10), 2895–2899.
(23) Ferguson, K. M. *Annu. Rev. Biophys.* **2008**, *37*, 353–373.
(24) Sorkin, A.; Goh, L. K. *Exp. Cell Res.* **2009**, *315*, 683–696.